Int. J. Mech. Sci. Vol. 28, No. 9, pp. 591–598, 1986
Printed in Great Britain.
0020-7403/86 $3.00 + .00

FULLY PLASTIC ASYMMETRIC CRACK GROWTH NEAR A SINGLE SHEAR BAND

G. A. KARDOMATEAS*
Massachusetts Institute of Technology, Cambridge, MA 02139, U.S.A.

Abstract—An asymmetric configuration may arise if a crack is near a weld or shoulder. In this case, loading into the plastic range can give a single asymmetric shear band extending from the crack tip instead of the two shear zones of the symmetric case. The resulting crack propagation near the active slip band, into previously pre-strained material, may give less ductility than the typical symmetric case where the crack advances into relatively unstrained material between the two shear zones. An approximate solution for the growth of such asymmetric cracks in regions dominated by an HRR type strain singularity is presented. The effect of strain hardening on crack growth is investigated and the predicted growth rate is compared with test data on several alloys.

NOTATION

- c crack advance distance
- u_i initiation displacement
- u_s far field displacement
- F_t hole growth ratio
- J path independent (J) integral
- k shear strength
- M^p Mode I mixity parameter
- n strain-hardening exponent
- W work per unit volume
- ε_{ij} strain components
- γ principal shear strain
- γ_f critical fracture strain
- η damage
- θ_s shear band orientation
- θ_f average crack growth angle
- θ_c cracking angle
- ξ current crack length
- ρ mean inclusion spacing
- σ_{ij} stress components
- σ_1 flow stress at unit strain
- σ mean normal stress
- τ principal shear stress
- ω crack opening angle

INTRODUCTION

In symmetric singly grooved tensile specimens the crack advances into the relatively undamaged region between two symmetric shear zones. In the fully plastic case, these zones narrow into bands that traverse the section, see Refs [1, 2]. Consider now the plane strain, singly grooved configuration of Fig. 1. The presence of a weld fillet or a harder, heat-affected zone on one side of the crack suppresses one of the two slip bands that would appear in a symmetrical specimen. This is likely to give asymmetric cracking near the remaining active slip line, with less ductility because the crack is advancing into pre-strained and pre-damaged

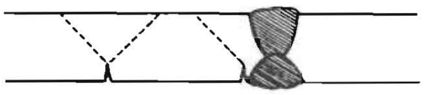

FIG. 1. Symmetric and asymmetric shear band configurations.

* Present address: General Motors Research Laboratories, Engineering Mechanics Department, Warren, MI 48090-9055, U.S.A.

material. Another indication of the reduced ductility is the fracture forming a shear lip as preliminary tensile tests have shown [3]. Near the tip of the growing crack, strain hardening will cause the deformation field to fan out. To model the stress and strain around the tip, one can use the dominant singularity solution for the mixed mode stationary crack problem that was developed by Shih [4] by extending the HRR [1, 2] singularity for the general mixed mode case. Microscopic observations have shown [3] that damage in these specimens is caused by hole growth from inclusions. Thus, as for a fracture criterion, that of McClintock *et al.* [5] will be used. The objective of this paper is to present a solution, based on the integration of the mixed mode HRR fields, for the growth of cracks near a single shear band.

ANALYSIS

Initiation

Consider a fracture running at an average angle θ_f with the shear band, as shown in Fig. 2, with a relative displacement u_s at an angle θ_s being imposed upon it by the far field conditions. Assume that the fracture strain is large compared to the yield strain, so that fully plastic conditions prevail. The fracture criterion is taken to be that the damage at some fracture process distance ρ reaches a critical value of unity. The direction of the crack will be through the point at which the least far-field displacement is required for unit damage. Assume that the crack abruptly jumps to the damaged site, and that sliding off occurs by the amount of the crack tip displacement required to attain the unit damage. The combination of cracking and sliding off gives the two new surfaces of the macro fracture. The process is then repeated. For a material law of the form:

$$\sigma = \sigma_1 \varepsilon^n, \tag{1}$$

where σ_1 is the flow stress at unit strain and n is the strain-hardening exponent, the local stress and strain fields, relative to the preceding crack direction θ_f are given in terms of the J integral and the Mode I mixity parameter as [4]:

$$\frac{\sigma_{ij}(r, \theta_c - \theta_f, M^P)}{\sigma_1} = \left(\frac{J}{\sigma_1 I_{1/n}(M^P) r}\right)^{n/(n+1)} \tilde{\sigma}_{ij}(\theta_c - \theta_f, M^P), \tag{2}$$

$$\varepsilon_{ij}(r, \theta_c - \theta_f, M^P) = \left(\frac{J}{\sigma_1 I_{1/n}(M^P) r}\right)^{1/(n+1)} \tilde{\varepsilon}_{ij}(\theta_c - \theta_f, M^P), \tag{3}$$

$$\frac{u_i}{r} = \left(\frac{J}{\sigma_1 I_{1/n}(M^P) r}\right)^{1/(n+1)} \tilde{u}_i(\theta_c - \theta_f, M^P), \tag{4}$$

where θ_c is the unknown and temporarily assumed critical orientation for maximum damage. The dimensionless functions $\tilde{\sigma}_{ij}$, $\tilde{\varepsilon}_{ij}$ and $I(n, M^P)$ have been numerically determined in [4] for $n = 1/3$ and $1/13$. The dimensionless functions $\tilde{u}_i$ can be derived by integrating the strain functions [6]. The mixity parameter, M^P, can also be determined if the relative flank-to-flank displacement of the singular field and the far slip line are assumed to be in the same direction. The path independent integral, J, can be evaluated in terms of the shear strength k, the far field displacement u_s and the shear band orientation θ_s. From its definition, for the crack

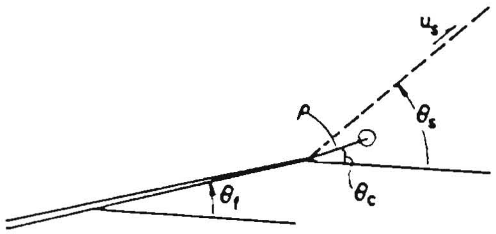

FIG. 2. Satisfying a crack growth criterion at a process radius ρ and a critical angle θ_c.

parallel to the x_1-direction

$$J = \int W\,dx_2 - T_j \frac{\partial u_j}{\partial x_1}\,ds, \tag{5}$$

where T_j is the traction vector and u_j is the displacement vector on Γ, s is the arc length and W is the work per unit volume. To obtain an expression for J, the simple formula from non-hardening plasticity for the work per unit volume is used in terms of the shear strain, γ, and the shear strength k:

$$W = k\gamma. \tag{6}$$

If Γ is chosen to be the outer boundary (Fig. 3), the tractions are zero everywhere except at the grips, where the displacement is constant, so $\partial u_j/\partial x_1 = 0$. Thus, the only contribution in the J integral comes from the first term. For a relative displacement u_s across the shear band of infinitesimal width δt:

$$\gamma = \frac{u_s}{\delta t}. \tag{7}$$

Noticing that $dx_2 = \delta t/\cos(\theta_s - \theta_f)$ the following is obtained:

$$J = ku_s/\cos(\theta_s - \theta_f), \tag{8}$$

where u_s is the magnitude of the far field shear displacement and θ_s is the direction of the far field band. Assume cracking to the new site (ρ, θ_c) followed by sliding off. When the process is repeated as shown in Fig. 4, the upper surface consists entirely of 'cracked' material, whereas the lower surface consists of a mixture of sheared off and cracked material. The angle of the 'upper' surface is

$$\theta_u = \theta_c. \tag{9}$$

The angle of the 'lower' surface is found from

$$\theta_l = \tan^{-1}\frac{\rho\sin\theta_c + u_s\sin\theta_s}{\rho\cos\theta_c + u_s\cos\theta_s}. \tag{10}$$

The average fracture direction is then

$$\theta_f = (\theta_l + \theta_c)/2. \tag{11}$$

The original assumption for the average fracture direction can now be checked and the entire process repeated until convergence. One might guess, for example, initially $\theta_f = \theta_s$ and $\theta_f = 0$.

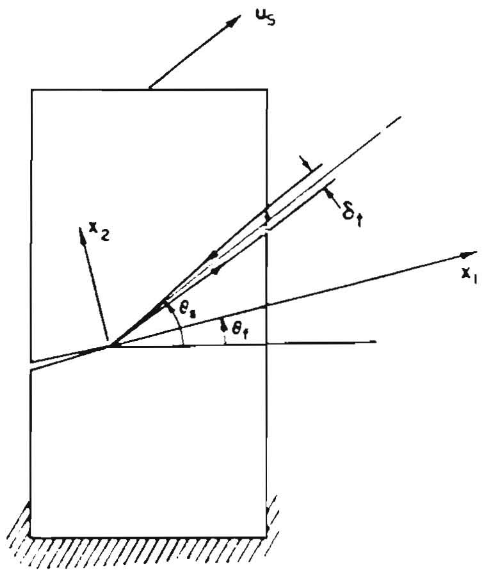

FIG. 3. Shear band parameters.

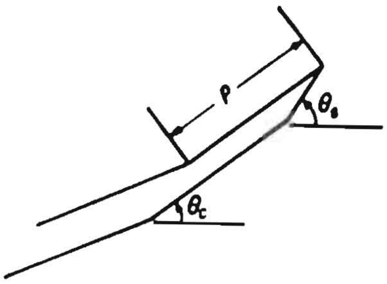

FIG. 4. Upper and lower faces of fracture surface.

To solve for the initiation conditions, a fracture criterion is needed. The critical strain for fracture can be calculated by using the fracture criterion of McClintock *et al.* [5] by which it is postulated that fracture due to micro-void coalescence occurs when the damage, η, reaches a value of unity. The damage is expressed in terms of a hole growth ratio, F_t, the principal shear strain, γ, and the triaxiality, σ/τ:

$$\eta = \frac{1}{\ln F_t}\left[\ln\sqrt{1+\gamma^2} + \frac{\gamma}{2(1-n)}\sinh\frac{(1-n)\sigma}{\tau}\right], \tag{12}$$

where the triaxiality can be written in terms of the angular stress functions (being tabulated in [4]) as:

$$\sigma/\tau = (\tilde{\sigma}_{rr} + \tilde{\sigma}_{\theta\theta})/2\tilde{\tau}, \tag{13}$$

with

$$\tilde{\tau} = \left[\tilde{\sigma}_{r\theta}^2 + \left(\frac{\tilde{\sigma}_{rr} - \tilde{\sigma}_{\theta\theta}}{2}\right)^2\right]^{1/2}. \tag{14}$$

The damage was considered at points a distance ρ ahead of the crack tip and the critical direction, θ_c, that requires the minimum far-field displacement for unit damage as well as the critical fracture stain, γ_f, and initiation displacement, u_i, was determined. For a shear band orientation at $\theta_s = 45°$ and with $\sigma_1/k = 3$, mean inclusion spacing $\rho = 10$ μm, hole growth factor $F_t = 1.3$, the above analysis was implemented for two strain-hardening exponents: $n = 1/13$ and $1/3$. For $n = 1/13$, it resulted in an average crack growth direction of $\theta_f = 36.3°$, and an initiation displacement $u_i/\rho = 0.714$. For the case $n = 1/3$, the corresponding findings were $\theta_f = 36.0°$ and $u_i/\rho = 0.758$. We turn now to the problem of predicting the crack growth.

Crack growth

Now the crack is growing steadily along the θ_f-direction. Assume that the crack is currently at the position c. At a position dc ahead of the crack the shear strain is:

$$\gamma_f + \left(\frac{\partial\gamma}{\partial r}\right)_c dc$$

where the subscript c refers to the current position of the crack. Notice that $(\partial\gamma/\partial r)_c$ is negative since the strain decreases ahead of the crack. So for the crack to advance by dc, a strain increment of

$$-\left(\frac{\partial\gamma}{\partial r}\right)_c dc$$

must be applied which is made up by the displacement required for further growth by ρ, i.e.

$$-\left(\frac{\partial\gamma}{\partial r}\right)_c dc = \left(\frac{\partial\gamma}{\partial u_s}\right)_{r=\rho} du_s. \tag{15}$$

The value of $(\partial\gamma/\partial r)$ is found by integrating the strain gradients produced by previous displacements. It is convenient to use the previous crack length ξ as the variable of integration:

$$\left(\frac{\partial\gamma}{\partial r}\right)_c = \left(\frac{\partial\gamma}{\partial r}\right)_i + \int_0^c \frac{d}{du_s}\left(\frac{\partial\gamma}{\partial r}\right)_\xi \left(\frac{\partial u_s}{\partial \xi}\right) d\xi, \tag{16}$$

where the subscript i refers to the value at crack initiation. From (3) and (8),

$$\left(\frac{\partial\gamma}{\partial r}\right)_i = \left(\frac{ku_i}{\sigma_1 I_{1/n}(M^P)(c+\rho)\cos(\theta_s-\theta_c)}\right)^{1/(n+1)} \frac{\tilde{\gamma}}{(n+1)(c+\rho)}. \tag{17}$$

An expression for the value of u_i can be found by using (8) and setting $r = \rho$ and $\gamma = \gamma_f$ in (3):

$$u_i = \frac{\sigma_1 I_{1/n}(M^P)\rho\cos(\theta_s-\theta_f)}{k}\left(\frac{\gamma_f}{\tilde{\gamma}}\right)^{n+1}. \tag{18}$$

In a similar way,

$$\frac{\partial\gamma}{\partial u_s} = \left(\frac{ku_s}{\sigma_1 I_{1/n}(M^P)r\cos(\theta_s-\theta_c)}\right)^{1/(n+1)} \frac{\tilde{\gamma}}{(n+1)u_s} \tag{19}$$

and

$$\frac{d}{du_s}\left(\frac{\partial\gamma}{\partial r}\right) = \left(\frac{ku_s}{\sigma_1 I_{1/n}(M^P)r\cos(\theta_s-\theta_c)}\right)^{1/(n+1)} \frac{\tilde{\gamma}}{(n+1)^2 r u_s}. \tag{20}$$

Substituting in equation (16) and using (15), (17), (19) and (20) the following equation for the displacement rate function $du_s^{1/(n+1)}/dc$ is obtained:

$$\frac{du_s^{1/(n+1)}}{dc} = \left(\frac{\rho}{c+\rho}\right)^{1/(n+1)} \frac{u_i^{1/(n+1)}}{(n+1)(c+\rho)} + \int_0^c \left(\frac{\rho}{c+\rho-\xi}\right)^{1/(n+1)} \frac{1}{(n+1)(c+\rho-\xi)} \frac{\partial u_s^{1/(n+1)}}{\partial \xi} d\xi. \tag{21}$$

Rename the variables by normalizing with respect to the mean inclusion spacing ρ,

$$C = c/\rho, \quad \Xi = \xi/\rho, \quad U = u_s/\rho.$$

and the following Volterra integral equation of the second kind is obtained:

$$\frac{dU^{1/(n+1)}}{dC} = \left(\frac{1}{C+1}\right)^{1/(n+1)} \frac{U_i^{1/(n+1)}}{(n+1)(C+1)} + \int_0^C \left(\frac{1}{C+1-\Xi}\right)^{1/(n+1)} \frac{1}{(n+1)(C+1-\Xi)} \frac{\partial U^{1/(n+1)}}{\partial \Xi} d\Xi. \tag{22}$$

This integral equation can be solved numerically for $dU^{1/(n+1)}/dC$ and the displacement is then found from

$$U(C) = \left[U_i^{1/(n+1)} + \int_0^C (dU^{1/(n+1)}/d\Xi)\,d\Xi\right]^{n+1}. \tag{23}$$

Calling the rate function $dU^{1/(n+1)}/dC$ constant provides a lower bound solution of:

$$dU^{1/(n+1)}/dC = U_i^{1/(n+1)}/(n+1)(C+1), \tag{24}$$

which integrates to:

$$U = U_i\left[\frac{\ln(C+1)}{n+1} + 1\right]^{n+1}. \tag{25}$$

RESULTS AND DISCUSSION

The numerical solution of the above integral equation (22) was performed via the Runge–Kutta method. Figure 5 shows how the displacement u_s increases with crack growth for the two strain-hardening exponents that have been considered here. The crack growth rate dC/dU vs crack advance C is shown in Fig. 6. After growth by $C = c/\rho = 400$, the lower hardening $n = 1/13$ case shows an 81% bigger growth rate than the high hardening $n = 1/3$ case. The expression (25) shows the same dependence on strain hardening but can only be used to give an upper bound to the growth rate.

The increasing crack growth per unit displacement (associated with the strain distribution flattening out in front of the crack at a decreasing rate) leads to size effects which can be estimated from the curves in Fig. 6. It can be observed, for example, that the crack growth per unit displacement after growth by $c/\rho = 400$ is 60% bigger than after growth by $c/\rho = 100$ for $n = 1/13$ but only 31% bigger for $n = 1/3$. The increasingly higher crack growth rate with less hardening is the cause of the loss of stability that had been observed in preliminary experiments [3] (the latter also depends on the compliance of the surrounding structure).

The fracture geometry in these asymmetric cracks can provide a relation between the more commonly used crack opening angle, ω, and the crack advance per unit far field displacement, dC/dU. In terms of the axial displacement $u_a = u_s \sin\theta_s$ (Fig. 7)

$$\omega = du_a \cos\theta_f/dc = \sin\theta_s \cos\theta_f/(dC/dU). \tag{26}$$

The higher growth rate in the low hardening case corresponds thus to a smaller crack opening angle.

Finally, the results can be compared with the quasi-steady solution for the low hardening case [7] which gave a growth rate 35% less than the more exact solution presented here. A normalized measure of the deviation from the steady state is given by:

$$u_s^* = \frac{c d^2 u_s/dc^2}{du_s/dc}. \tag{27}$$

For the cases considered, this parameter is practically constant during crack growth, $u_s^* = -0.27$ for $n = 1/13$ and $u_s^* = -0.18$ for $n = 1/3$, reflecting a more steady growth for the higher hardening case.

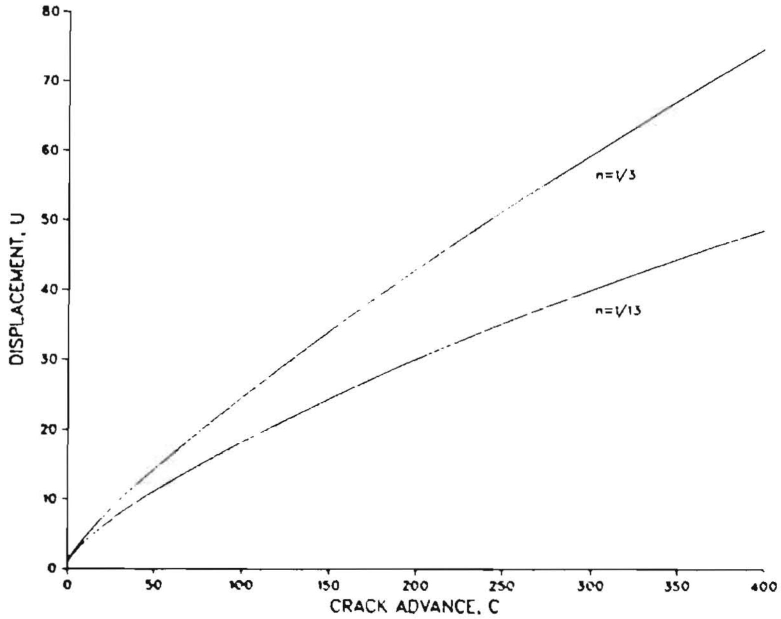

FIG. 5. Displacement $U = u_s/\rho$ vs crack growth $C = c/\rho$.

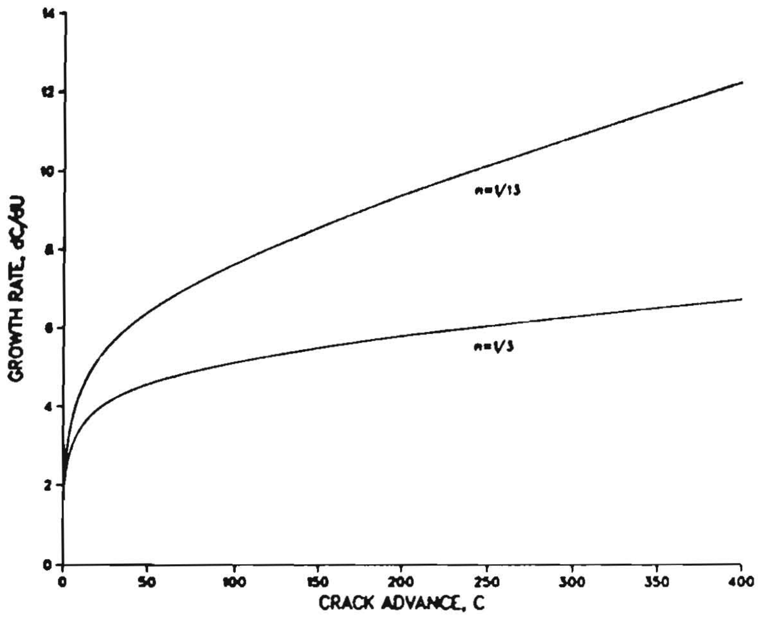

FIG. 6. Crack growth rate dC/dU vs crack growth $C = c/\rho$.

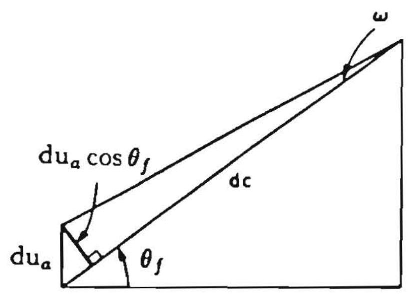

FIG. 7. Deriving the relation between the crack opening angle and the crack growth rate.

EXPERIMENTAL OBSERVATIONS

Tests were performed on fatigue-pre-cracked asymmetric specimens [3] (asymmetry provided through a machined shoulder) of the lower hardening HY80 and HY100 steel ($n \simeq 0.10$) and the higher hardening A36 hot rolled and 1018 normalized steel ($n \simeq 0.24$). In these tests, in addition to the load–displacement data, the topographies of the crack path were plotted using a travelling stage microscope. These fracture surface profiles allow determining the initiation and growth displacements, the crack orientation θ_f and the crack opening angle ω.

Results from these tests are summarized in Table 1. Crack growth orientations were found within 2° of 38° from the transverse. The smaller than 45° angle was expected from the higher triaxiality [4]. The initiation displacement is one order of magnitude bigger than the predicted one (order of inclusion spacing ρ) due to the presence of blunting. Blunting is expected to affect the local field at initiation by raising the strains but limiting the triaxiality [8]. During growth, however, the fracture surface profiles show a clearly defined crack opening angle [3].

Concerning now the experimentally measured crack growth rate and crack opening angle, a good agreement was achieved with the predicted ones [for the specimen ligament of $C = c/\rho = 250$, $dC/dU = 10.1$ for $n = 1/13$ and $dC/dU = 6.0$ for $n = 1/3$ from Fig. 6; the crack opening angle of 3.2 and 5.5°, respectively, is found by using equation (26)].

TABLE 1. TEST DATA

Alloy	Experimental		Predicted
	Low hardening ($n \simeq 0.10$)		$n = 1/13$
	HY 80	HY 100	
u_i/ρ	18	13	0.714
θ_f	40°	40°	36.3°
$(dc/du)_{max}$	10.4	9.5	10.1
ω	2.1°	2.4°	3.2°
	High hardening ($n \simeq 0.24$)		$n = 1/3$
	A36 HR	1018 norm.	
u_i/ρ	27	38	0.758
θ_f	38°	38°	36.0°
$(dc/du)_{max}$	5.5	4.6	6.0
ω	5.0°	6.0°	5.5°

Furthermore, it should be noted that the asymmetric specimens are less ductile than the corresponding symmetric ones [3] (crack growth rate larger by a factor ranging from 1.2 to 3, the higher growth rate with less hardening). In this paper, however, the attention is focused on predicting the growth of the asymmetric cracks.

CONCLUSIONS

A solution based on the integration of the stationary mixed mode crack tip singularities was presented for the growth of fully plastic asymmetric cracks near a single shear band. Assuming that near tip fields follow a power law asymptotic behavior, gives the crack growth rate as a solution of an integral equation. The analysis provides also the direction of the growing crack and the initiation displacement. Two strain-hardening exponents, $n = 1/13$ and $1/3$, were considered. A higher growth rate (and smaller crack opening angle) is predicted for less hardening. The crack growth per unit displacement increases as the crack advances, the increase being steepest for a lower strain hardening. The increasingly higher growth rate of such asymmetric cracks in the lower hardening alloys leads to increased stiffness requirements for stable fracture. The results of the analysis appear plausible when compared to test data on several alloys.

Acknowledgements—The financial support of the Office of Naval Research, Arlington, Virginia, Contract N0014-82K-0025 with the Massachusetts Institute of Technology, is gratefully acknowledged.

REFERENCES

1. J. W. HUTCHINSON, Singular behavior at the end of a tensile crack in a hardening material. *J. Mech. Phys. Solids* **16**, 13 (1968).
2. J. R. RICE and G. F. ROSENGREN, Plane strain deformation near a crack tip in a power-law hardening material. *J. Mech. Phys. Solids* **16**, 1 (1968).
3. G. A. KARDOMATEAS, Mixed Mode I and II Fully Plastic Crack Growth from Simulated Weld Defects, Ph.D. thesis, Dept of Mechanical Engineering, Massachusetts Institute of Technology (1985).
4. C. F. SHIH, Small scale yielding analysis of mixed mode plane strain crack problems. *Fracture Analysis, ASTM Am. Soc. Test. Mat., Philadelphia STP* **560**, 187 (1974).
5. F. A. MCCLINTOCK, S. M. KAPLAN and C. A. BERG, Ductile fracture by hole growth in shear bands. *Int. J. Fract. Mech.* **2**, 614 (1966).
6. G. A. KARDOMATEAS, Displacement fields for mixed mode elastic plastic cracks. To appear in *Engng Fract. Mech.* (1986).
7. G. A. KARDOMATEAS, A model for quasi-steady asymmetric fully plastic crack growth. *Int. J. Pres. Ves. and Piping* **19**, 237 (1985).
8. J. R. RICE and M. A. JOHNSON, The role of large crack tip geometry changes in plane strain fracture. In *Inelastic Behavior of Solids* (Edited by M. F. KANNINEN), p. 641. McGraw-Hill, New York (1970).